




**Nuclear matrix elements for neutrinoless  $\beta\beta$  decays and spin-dipole giant resonances**Hiroyasu Ejiri \**Research Center for Nuclear Physics, Osaka University, Osaka 567-0047, Japan*Lotta Jokiniemi *Department of Quantum Physics and Astrophysics and Institute of Cosmos Sciences, University of Barcelona, Barcelona 08028, Spain*Jouni Suhonen *Department of Physics, University of Jyväskylä, Jyväskylä FI-40014, Finland*

(Received 12 October 2021; accepted 24 January 2022; published 9 February 2022)

Nuclear matrix element (NME) for neutrinoless  $\beta\beta$  decay (DBD) is required for studying neutrino physics beyond the standard model by using DBD. Experimental information on nuclear excitation and decay associated with DBD is crucial for theoretical calculations of the DBD-NME. The spin-dipole (SD) NME for DBD via the intermediate SD state is one of the major components of the DBD-NME. The experimental SD giant-resonance energy and the SD strength in the intermediate nucleus are shown for the first time to be closely related to the DBD-NME and are used for studying the spin-isospin correlation and the quenching of the axial-vector coupling, which are involved in the NME. So they are used to help the theoretical model calculation of the DBD-NME. Impact of the SD giant resonance and the SD strength on the DBD study is discussed.

DOI: [10.1103/PhysRevC.105.L022501](https://doi.org/10.1103/PhysRevC.105.L022501)

Neutrinoless  $\beta\beta$  decay (DBD), which violates the lepton-number conservation law, is a sensitive and realistic probe for studying the neutrino ( $\nu$ ) nature (Majorana or Dirac) relevant to the origin of matter in the universe, the absolute  $\nu$ -mass scale, and other  $\nu$  properties beyond the standard model [1–3]. The nuclear matrix element (NME) for the neutrinoless DBD is crucial to extract the effective  $\nu$  mass and other  $\nu$  properties of the particle physics interests from the decay rate. The NME is also needed to design DBD detectors [4–6]. Thus the NMEs are of great interest from astro-, particle, and nuclear physics view points. Theoretical works on DBD-NMEs by using various nuclear models are discussed in Refs. [7–12] and recent DBD experiments in Refs. [13–15].

Actually, accurate theoretical calculations for the DBD-NME are very hard since they are sensitive to nucleonic and non-nucleonic correlations and nuclear medium effects. Consequently, calculated DBD-NMEs, including the effective axial-vector coupling ( $g_A$ ), scatter over an order of magnitude [3,6] depending on the nuclear models, the interaction parameters, and the effective coupling ( $g_A^{\text{eff}}$ ) used in the models. Thus experimental inputs are useful to check the theoretical models and the nuclear parameters to be used for the models [1,6].

The present letter aims to show for the first time that the experimental energy and the strength of the spin-dipole (SD) giant resonance in the intermediate nucleus are closely related to the DBD-NME ( $M^{0\nu}$ ) based on the proton-neutron quasiparticle random-phase approximation (pnQRPA) model

and reflect the nuclear structure and the quenching of the  $g_A$ , which are involved in the DBD-NME. Here the SD strength is given as  $B^-(\text{SD}) = |M^-(\text{SD})|^2$  with  $M^-(\text{SD})$  being the SD NME. We note that  $M^-(\text{SD})$  is associated with the SD component of the DBD-NME, which is one of the major components of the DBD-NME, and the quenching of  $g_A$  is one of key parameters for the theoretical model calculation. Thus experimental information on the SD giant-resonance energy  $E_G(\text{SD})$  and the SD strength  $B^-(\text{SD})$  are used to help and check the theoretical model calculation of the DBD-NME.

Recently, the experimental  $E_G(\text{SD})$  values were shown to depend on the isospin  $z$  component  $T_z = (N - Z)/2$  with  $N$  and  $Z$  being the neutron and proton numbers [6], and pnQRPA calculations for  $M^{0\nu}$  were performed by adjusting the particle-hole parameter to the  $E_G(\text{SD})$  in Ref. [12], where  $g_A^{\text{eff}} = 1$  is assumed. Single- $\beta$  SD NMEs for the ground states in the medium-heavy nuclei (mostly non-DBD nuclei) were studied in the framework of the pnQRPA and were found to be reduced by  $g_A^{\text{eff}}/g_A \approx 0.5$ , depending much on the individual states [16].

The present paper puts emphasis on studying and discussing universal features in the  $E_G(\text{SD})$ , the GT and SD strengths, and the  $M^{0\nu}$  as a function of the mass number  $A$ . For  $M^{0\nu}$ , we use a common value for the  $g_A^{\text{eff}}$  as derived by referring to the experimental summed GT strengths for the DBD nuclei and the SD NMEs for the ground-state transitions in the medium-heavy nuclei. Then we discuss impact of the present findings on the DBD experiments.

We discuss  $\beta^-\beta^-$  decays of the ground-state-to-ground-state transition of  $0^+ \rightarrow 0^+$ . The neutrinoless DBD ( $0\nu\beta\beta$ )

\*ejiri@rcnp.osaka-u.ac.jp

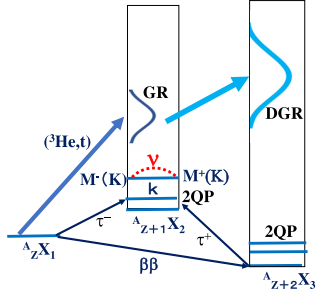


FIG. 1. DBD transition scheme for  ${}^A_Z X_1 \rightarrow {}^A_{Z+2} X_3$  with the Majorana  $\nu$  exchange in the intermediate nucleus  ${}^A_{Z+1} X_2$ .  $\tau^+$  and  $\tau^-$ : Isospin raising and lowering operators.  $M^-(K)$  and  $M^+(K)$ :  $\tau^-$  and  $\tau^+$  K-mode NMEs associated with the K-mode DBD NME.  $k$ : Intermediate state.  $({}^3\text{He}, t)$ : Charge-exchange reaction. 2QP: Two-quasiparticle state. GR: Giant resonance. DGR: Double giant resonance. See text.

for  ${}^A_Z X_1 \rightarrow {}^A_{Z+2} X_3$  is schematically shown in Fig. 1. The intermediate nucleus is  ${}^A_{Z+1} X_2$ . The  $0\nu\beta\beta$  process to be discussed is the Majorana  $\nu$ -mass process of the current interest. Here a light Majorana  $\nu$  is virtually exchanged between two neutrons in the DBD nucleus. DBD nuclei discussed are medium-heavy ( $A = 76\text{--}136$ ) nuclei with the high  $\nu$ -mass sensitivity [14]. The DBD rate is expressed as in Refs. [1,3,6].

$$R^{0\nu} = \ln 2 g_A^4 G^{0\nu} [m_{\beta\beta} |M^{0\nu}|]^2, \quad (1)$$

where  $G^{0\nu}$  is the phase-space factor,  $g_A = 1.27$  is the axial-vector coupling for a free nucleon in units of the vector coupling of  $g_V$ ,  $m_{\beta\beta}$  is the effective  $\nu$  mass, and  $M^{0\nu}$  is the DBD NME. The NME is given as [3,6,7,12]

$$M^{0\nu} = \left(\frac{g_A^{\text{eff}}}{g_A}\right)^2 [M_{\text{GT}}^{0\nu} + M_T^{0\nu}] - \left(\frac{g_V}{g_A}\right)^2 M_F^{0\nu}, \quad (2)$$

where  $M_{\text{GT}}^{0\nu}$ ,  $M_T^{0\nu}$ , and  $M_F^{0\nu}$  are the axial-vector [Gamow-Teller (GT)], tensor (T) and vector [Fermi (F)] DBD-NMEs, respectively, and  $g_A^{\text{eff}}$  is the effective axial-vector coupling introduced to incorporate the quenching effect.

DBDs involve mainly axial-vector spin-isospin ( $\sigma\tau$ ) and vector isospin ( $\tau$ ) transitions. The NMEs depend much on nucleonic and non-nucleonic  $\sigma\tau$  and  $\tau$  interactions and their correlations. The pnQRPA model, which includes explicitly the nucleonic interactions and their correlations, has been widely used. Then the NMEs  $M_\alpha^{0\nu}$  with  $\alpha = \text{GT}, \text{T}, \text{F}$  are given by the pnQRPA model NMEs, and  $g_A^{\text{eff}}/g_A$  stands for the renormalization (quenching) coefficient due to the non-nucleonic  $\sigma\tau$  correlations, nuclear medium effects, and others which are not explicitly included in the pnQRPA model. Then  $g_A^{\text{eff}}/g_A$  depends on the model to be used and the experimental data to be compared with, as discussed in Refs. [4,6,16–20]. In particular, the present pnQRPA is the one which is standardly used in the  $\beta$  and  $\beta\beta$  calculations, and it is explained in great detail in Ref. [21]. The  $g_V = 1$  for a free nucleon is assumed in Eq. (2).

The NME  $M_\alpha^{0\nu}$  is given by the sum of the NMEs  $M_\alpha^{0\nu}(k)$  for the intermediate states  $k$  as [3,6,7,12]

$$M_\alpha^{0\nu} = \sum_k M_\alpha^{0\nu}(k), \quad M_\alpha^{0\nu}(k) = \langle T_\alpha(k) \rangle, \quad (3)$$

where the transition operator  $T_\alpha(k)$  with  $\alpha = \text{GT}, \text{T},$  and  $\text{F}$  are given by  $T_{\text{GT}}(k) = t^\pm \sigma h_{\text{GT}}(r_{12}, E_k) t^\pm \sigma$ ,  $T_T(k) = t^\pm h_T(r_{12}, E_k) S_{12} t^\pm$ , and  $T_F(k) = t^\pm h_F(r_{12}, E_k) t^\pm$ . The operator includes the neutrino potential  $h_\alpha(r_{12}, E_k)$  with  $r_{12}$  being the distance between the two neutrons involved in the  $\nu$  exchange and  $E_k$  the excitation energy of the intermediate state  $k$ ,  $S_{12}$  the spin tensor operator, and  $t^\pm$  the isospin operators for proton  $\rightleftharpoons$ neutron. Since the momentum of the virtual  $\nu$  is of the order of  $1/r_{12} \approx 100 \text{ MeV}/c$ , the NME involves mainly intermediate states  $k$  in the wide ranges of the spins of  $J^\pi \approx 0^\pm\text{--}7^\pm$  and  $E_k \approx 0\text{--}30 \text{ MeV}$ . Thus, the DBD-NME may reflect gross properties of the nuclear core.

The axial-vector SD ( $J^\pi = 2^-$ ) component of the  $M_{\text{GT}}^{0\nu}(\text{SD})$  in Eq. (2) is one of the major components since the orbital angular momentum matches the medium momentum of the virtual neutrino. The SD DBD-NME is associated with the product of the single  $\tau^\pm$  SD NMEs of  $M^+(\text{SD})$  and  $M^-(\text{SD})$ , as shown in Fig. 1. The single- $\beta$  SD NMEs are expressed as  $M^\pm(\text{SD}) = (t^\pm [\sigma f(r) Y_1]_2)$  with  $Y_1$  being the spherical harmonics.

On the other hand, the two-neutrino DBD within the standard model is followed by the emission of the two real  $s$ -wave ( $l = 0$ ) neutrinos with low momentum, and the NME ( $M^{2\nu}$ ) involves exclusively the  $M^\pm(\text{GT})$  for GT  $1^+$  intermediate states at the low excitation-energy region. Thus  $M^{2\nu}$  is very sensitive to properties of the valence nucleons at the proton neutron Fermi surfaces. So far, most theoretical DBD models use these valence-nucleon GT properties.

Recent experimental studies on DBD-NMEs are in Refs. [6,15]. Among them the charge-exchange  $({}^3\text{He}, t)$  reactions provide useful information on  $M^-(\text{K})$  with  $\text{K} = \text{GT}, \text{SD}$ , and so on, for DBD nuclei  $A = 76\text{--}136$  in wide excitation-energy and momentum regions, which are relevant to DBD-NMEs [19,22–30]. We discuss the experimental results on the DBD nuclei  ${}^{76}\text{Ge}$ ,  ${}^{96}\text{Zr}$ ,  ${}^{100}\text{Mo}$ ,  ${}^{116}\text{Cd}$ ,  ${}^{128}\text{Te}$ ,  ${}^{130}\text{Te}$ , and  ${}^{136}\text{Xe}$ . As an example of the reactions, Fig. 2 shows the  ${}^{100}\text{Mo}$  spectrum [26].

The pnQRPA calculations for  $M^{0\nu}$  [12] were extended to study relation of the  $M^{0\nu}$  to the experimental  $E_{\text{GR}}(\text{SD})$  and the GT and SD strength distributions. The calculations were made for  $g_A^{\text{eff}}/g_A = 0.74$  and  $0.55$  by referring to the experimental data [6,16,19,31] (see (v)). The modified single-particle energies so as to reproduce the observed energies for low-lying states were used for all nuclei, except for  ${}^{116}\text{Cd}$  where the level energies based on the Woods-Saxon potential were used. The particle-particle interaction parameter  $g_{\text{pp}}$  is divided into isoscalar and isovector parts in order to recover the isospin symmetry (vanishing of the two-neutrino DBD Fermi NME) and to reproduce the observed  $M^{2\nu}$  [20]. The  $g_{\text{pp}}$  dependence of  $M^{2\nu}$  is visualized, e.g., in Ref. [32]. The particle-hole interaction  $g_{\text{ph}}$  derived so as to reproduce the experimental  $E_{\text{GR}}(\text{SD})$  in Ref. [6] was used for all multiple transitions except for the GT one, for which the  $g'_{\text{ph}}$  that

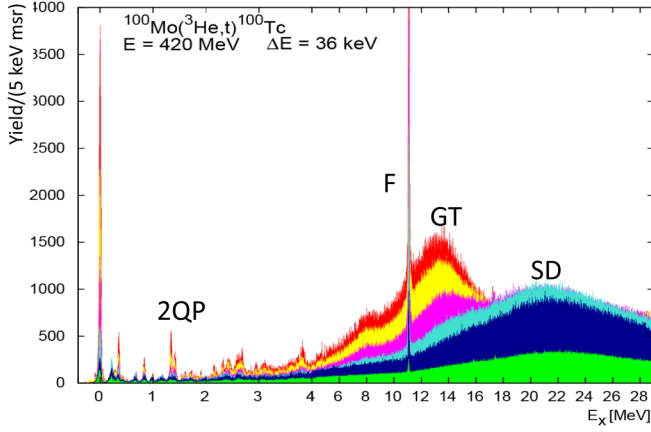


FIG. 2. The energy spectrum of the  $({}^3\text{He}, t)$  reaction on  ${}^{100}\text{Mo}$  [26]. F, GT, and SD are Fermi  $0^+$ , GT  $1^+$ , and SD  $2^-$  giant resonances, respectively. The energy scale below 4 MeV is enlarged to make the sharp peaks visible. The  $1^-$  and  $0^-$  giant resonances are at the higher-energy region of SD. 2QP: Two-quasiparticle states. Yields at the  $t$  emission angles of  $0^\circ$ – $0.5^\circ$ ,  $0.5^\circ$ – $1^\circ$ ,  $1^\circ$ – $1.5^\circ$ ,  $1.5^\circ$ – $2^\circ$ ,  $2^\circ$ – $2.5^\circ$ , and  $2.5^\circ$ – $3^\circ$ , each in degrees, are shown by red, yellow, pink, light blue, blue, and green, respectively. F and GT transitions are enhanced at the forward angles (red, yellow), while the SD ones at larger angles (blue, green).

fits the experimental  $E_G(\text{GT})$  was used. Actually, we first adjust  $g_{pp}$  using  $g_{ph} = 1$ . Then using the adjusted  $g_{pp}$ , we adjust  $g_{ph}$  to fit the GR energy. This is a common way to get the pp and ph interaction parameters to achieve a procedure which is the least prone to errors [20]. The parameter adjustments for the pnQRPA calculation are well described in Ref. [12].

Interesting universal features on the experimental SD data and the calculated NMEs are found as given below in (i)–(vi):

- (i) The GT  $1^+$  strength  $B^-(\text{GT}) = |M^-(\text{GT})|^2$  and the SD  $2^-$  strength  $B^-(\text{SD}) = |M^-(\text{SD})|^2$  are mostly concentrated, respectively, in the GT and SD giant resonances at the high-excitation-energy region in all nuclei (see Fig. 2). Several sharp peaks in the low-energy (0- to 6-MeV) region are 2QP states. The giant-resonance energies in units of MeV are found to be expressed as

$$E_G(\text{GT}) \approx 0.06A + 7.0, \quad E_G(\text{SD}) \approx 0.06A + 14.5, \quad (4)$$

as shown in Fig. 3(a). They are given also as  $E_G(\text{GT}) \approx 0.4T_z + 9$  MeV and  $E_G(\text{SD}) \approx 0.4T_z + 16.5$  MeV [6]. Note that  $A \approx 4(N - Z) + 28$  for the present nuclei. The  $E_G(\text{GT})$  and  $E_G(\text{SD})$  increase gradually as  $A$  and  $N - Z$  increase. This is in accord with the GT and SD giant resonances in other nuclei [33].

The energies are found to be shifted higher above the GT and SD 2QP states by  $E_S(\text{GT}) \approx 0.33(N - Z)$  MeV and  $E_S(\text{SD}) \approx 0.3(N - Z)$  MeV. They increase with increase of  $N - Z$  and  $A$ , which reflect the giant-resonance strengths. The SD giant-resonance energies are higher than the GT ones by around  $0.9 \hbar\omega$  (harmonic oscillator energy) because of the

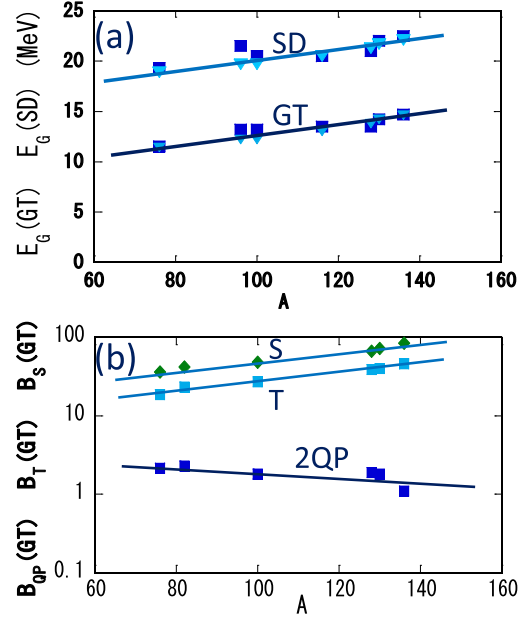


FIG. 3. (a) Experimental GT  $1^+$  and SD  $2^-$  giant-resonance energies of  $E_G(\text{GT})$  and  $E_G(\text{SD})$ . Solid lines: Fits by Eq. (4). Squares: The observed energies. Inverse triangles: The energies from the experimental  $E_G(\text{GT}) \approx 0.4T_z + 9$  MeV and  $E_G(\text{SD}) \approx 0.4T_z + 16.5$  MeV [6] as used in the pnQRPA. (b) The GT strengths in logarithmic scale. GT  $1^+$  strength  $B^-(\text{GT})$ :  $S$ :  $B_5^-(\text{GT})$  for the nucleon-based sum-rule limit.  $T$ :  $B_7^-(\text{GT})$  for the observed total strength up to  $E_G(\text{GT}) + 10$  MeV. The strength beyond  $E_G$  is corrected for the small contribution from the quasifree scattering. 2QP:  $B_{\text{QP}}^-(\text{GT})$  for the sum of the observed 2QP strengths up to 6 MeV. Straight lines are fits to the data.

$1 \hbar\omega$  jump involved in the SD excitation. The giant-resonance energies depend on  $A$  and  $N - Z$ , thus following the gross properties of nuclear core.

- (ii) The observed total GT strengths [ $B_7^-(\text{GT})$ ] increase as  $A$  and  $N - Z$  increase, and they are around 0.55 of the nucleon-based sum-rule limit of  $B_5^-(\text{GT}) \approx 3(N - Z)$  as shown in Fig. 3(b) [6]. These are consistent with GT strengths in other nuclei [33]. The reduction is incorporated by the quenched axial-vector coupling of  $g_A^{\text{eff}}/g_A \approx \sqrt{0.55} \approx 0.74$ . This may stand for such non-nucleonic effects that are not included in the simple sum rule. The 2QP GT states are expected in the low-excitation-energy region. The summed strength  $B_{\text{QP}}^-(\text{GT})$  up to 6 MeV is around 10–5% of the total strength of  $B_7^-(\text{GT})$  and decreases as  $A$  and  $N - Z$  increase [see Fig. 3(b)].

The GT and SD cross sections for the  $({}^3\text{He}, t)$  reactions show the maximum at the  $s$ - and  $p$ -wave  $t$  scattering angles of  $\theta = 0^\circ$  and around  $2^\circ$ , respectively. The GT and SD cross sections there are the same within 10%. The SD cross section for the 2QP states below the SD giant resonance is also nearly same as the GT one below the GT giant resonance. The SD cross sections for the 2QP region are found to be also of the order of 10–5% of the total SD

TABLE I. The pnQRPA NMEs.  $M_V^{0v} = (g_V/g_A)^2 M_F^{0v}$  and  $M_A^{0v} = (g_A^{\text{eff}}/g_A)^2 (M_{\text{GT}}^{0v} + M_T^{0v})$  and  $M^{0v}$  [see Eq. (2)]. Note that for  $^{100}\text{Mo}$  the  $0g$ -shell effect on the  $M^{2v}$  is huge but is small on the  $M^{0v}$ . Superscripts “ $a$ ” and “ $b$ ” denote the NMEs with  $g_A^{\text{eff}}/g_A = 0.74$  and  $0.55$ , respectively.

$^A X$	$M_V^{0v}$	$M_A^{0va}$	$M_A^{0vb}$	$M^{0va}$	$M^{0vb}$
$^{76}\text{Ge}$	-1.16	2.59	2.02	3.75	3.18
$^{96}\text{Zr}$	-1.03	2.12	1.29	3.14	2.31
$^{100}\text{Mo}$	-1.51	2.11	1.81	3.62	3.32
$^{116}\text{Cd}$	-1.01	2.03	1.43	3.03	2.44
$^{128}\text{Te}$	-0.95	1.88	1.29	2.82	2.24
$^{130}\text{Te}$	-0.81	1.57	1.08	2.37	1.89
$^{136}\text{Xe}$	-0.63	1.57	1.05	2.19	1.68

cross sections. Thus the SD strengths at the giant resonance and the 2QP region show the similar trends as the GT strengths there. The 2QP GT and 2QP SD strengths for the very low-excitation-energy (a few MeV) region depend on individual nuclei, reflecting the valence nucleon configurations containing single-particle states near the proton and neutron Fermi surfaces of each nucleus.

- (iii) The pnQRPA NMEs of  $M_A^{0v} = (g_A^{\text{eff}}/g_A)^2 [M_{\text{GT}}^{0v} + M_T^{0v}]$  and  $M^{0v}$  for  $g_A^{\text{eff}}/g_A = 0.74$  [see Eq. (2)] are shown in Table I. They are found to decrease gradually as  $A$  and  $N - Z$  increases, reflecting the gross properties of the nuclear core, as shown in Fig. 4. This is in contrast to the SD and GT giant-resonance energies and the strengths, which increase as functions of  $A$  and  $N - Z$  (see Fig. 3). The DBD-NMEs are found to behave like the 2QP GT and the 2QP SD strengths of  $B_{\text{QP}}^-(\text{GT})$  and  $B_{\text{QP}}^-(\text{SD})$  [see Fig. 3(b)].

$M^{2v}$ , which is associated with the GT NMEs for low-lying 2QP  $1^+$  states, changes more than a factor

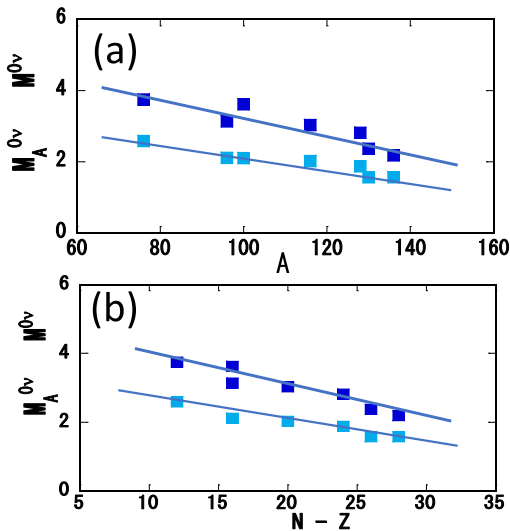


FIG. 4.  $M^{0v}$  (blue squares) and  $M_A^{0v}$  (light blue square) with  $g_A^{\text{eff}}/g_A = 0.74$  are plotted against (a)  $A$  and (b)  $N - Z$ . Solid lines are fits. See text.

10 among the DBD nuclei, depending on the valence nucleon configurations of states near the Fermi surfaces [6,34–36].

- (iv) The repulsive  $\tau\sigma$  interaction pushes up the GT and SD strengths to the GT and SD giant resonances and reduces the low-lying GT and SD NMEs with respect to the 2QP NMEs due to the  $\tau\sigma$  nuclear polarization effects [4,37,38]. The reduction rate is given by  $1/(1 + \chi)$  with  $\chi$  being the  $\tau\sigma$  susceptibility. Likewise, the DBD-NME  $M^{0v}$  may be doubly reduced by the factor  $[1/(1 + \chi)]^2$ . Then the NME may be expressed as  $M^{0v} \approx M_0^{0v}/(1 + \chi)^2$  with  $M_0^{0v} \approx 6.5$  and  $\chi \approx 0.025(N - Z)$  for the present DBD nuclei. As  $(N - Z)$  and  $A$  increase, the susceptibility  $\chi$  increases, and  $M^{0v}$  decreases. The value for  $\chi$  is around 0.4 for DBD nuclei with  $N - Z$  around 16, and  $M^{0v} \approx 0.5 M_0^{0v}$ .

The particle-hole interaction ( $g_{\text{ph}}$ ) pushes up the giant resonances in energy, shifting the spin-isospin strengths from the low-lying states to the giant resonances and reduces the DBD-NME  $M^{0v}$ . The susceptibility  $\chi$  in (iv) is proportional to  $g_{\text{ph}}$  [4,38]. Thus  $\chi$  increases as  $g_{\text{ph}}$  increases and  $M^{0v}$  decreases as  $g_{\text{ph}}$  increases, with 10% increase of  $g_{\text{ph}}$  leading to around 5 % decrease of  $M^{0v}$  in accord with the pnQRPA calculations [12].

- (v) We use for the present DBD NMEs ( $g_A^{\text{eff}}/g_A \approx 0.74$  and  $0.55$ , which are suggested, respectively, by comparing the observed total GT strength of  $B_T^-(\text{GT})$  and the GT and SD strengths for low-lying states with those of the sum rule and the pnQRPA model [6,16,19,30,31]. The charge-exchange reaction data show the uniform quenching factor over the momentum region of 30–120 MeV/ $c$  of the DBD interest [6,30]. The coupling of  $g_A^{\text{eff}} = 1$  (i.e.,  $g_A^{\text{eff}}/g_A = 0.79$ ) is used in Ref. [12]. The quenching of the  $g_A$  for  $M^{0v}$  is discussed in [6,17,19,39] and that for GT and the  $M^{2v}$  in Refs. [6,18,40–42]. The similar quenching factor is obtained for the low-momentum GT NMEs from the chiral two-body current [43].

- (vi) The NMEs  $M_A^{0v} = (g_A^{\text{eff}}/g_A)^2 [M_{\text{GT}}^{0v} + M_T^{0v}]$  with  $g_A^{\text{eff}}/g_A = 0.55$  are smaller than those with  $(g_A^{\text{eff}}/g_A) = 0.74$  by factors around 0.7. The reduction is less severe than 0.62 for the ratio  $(g_A^{\text{eff}}/g_A)^2$ . The difference is due to the dependence of the computed NME  $M^{2v}$  on the ratio  $g_A^{\text{eff}}/g_A$  and hence on  $g_{\text{pp}}$ . As  $g_A^{\text{eff}}/g_A$  decreases the magnitude of the experimental NME, derived from the experimental half-life, increases and hence also the magnitude of the computed NME has to increase. Since the magnitude of the computed  $M^{2v}$  increases with decreasing value of  $g_A^{\text{eff}}/g_A$  [32] the value of  $g_{\text{pp}}$  has to decrease. This, in turn, means that the NMEs  $M^{0v}$  are computed with different values of  $g_{\text{pp}}$  for different values of the ratio  $g_A^{\text{eff}}/g_A$  (larger ratio means larger value of  $g_{\text{pp}}$ ).  $M^{0v}$  behaves in a similar way in terms of  $g_A^{\text{eff}}/g_A$  as  $M^{2v}$  (less sensitively, though, since the higher multipoles are less dependent on the ratio  $g_A^{\text{eff}}/g_A$  than the  $1^+$  multipole). As shown in



Table I, the computed NMEs  $M^{0\nu}$  with  $g_A^{\text{eff}}/g_A = 0.55$  are smaller by factors around 0.8 than those with  $g_A^{\text{eff}}/g_A = 0.74$ .

Let us discuss the impact of the present findings on DBD studies. On the bases of the above discussions, we use  $g_A^{\text{eff}}/g_A \approx 0.65 \pm 0.1$ .  $M^{0\nu}$  with this  $g_A^{\text{eff}}/g_A$  region corresponds approximately to the  $\pm 10\%$  region around

$$M^{0\nu} \approx 5.2 - 0.023A, \quad M^{0\nu} \approx 4.2 - 0.08(N - Z). \quad (5)$$

The DBD NMEs for  $A = 76-136$  are considered to be around 3-2. Since they do not depend much on individual nuclei, selection of the DBD nucleus for the experiment may be made from experimental requirements such as the availability of ton-scale DBD isotopes, the large  $Q$  value, the low-background, and the high energy-resolution.

The present analyses show that the pnQRPA  $M^{0\nu}$  is closely related to the SD giant resonance and the distribution of the strength  $B^-(K) = |M^-(K)|^2$  with  $K = \text{GT}$  and  $\text{SD}$  in the intermediate nucleus. Various nuclear models are being used for calculating  $M^{0\nu}$ . Then it is interesting to compare the calculated strength distribution of  $B^-(K)$  in  ${}^A_{Z+1}\text{X}_2$  by using the model wave function for  ${}^A_{Z+1}\text{X}_1$  with the observed giant resonance and the strength.

Actually, the SD ( $J^\pi = 2^-$ ) giant resonance is accompanied at the higher-energy side by the resonances with  $J^\pi = 1^-, 0^-$  and the quasifree scattering. Further experimental studies for their strengths and also for higher multipole strengths with  $J^\pi = 3^+$  and  $J^\pi = 4^-$  are interesting. The low- and high-multipole giant resonances are studied in the pnQRPA [44].

Ordinary muon capture of ( $\mu, \nu_\mu$ ) is used to study  $M^+(K)$  [6,45]. The large strength is found in the giant resonances

[45,46]. The quenching of  $g_A$  in the muon strengths is under discussions [47,48]. Actually,  $\tau^\pm$  strengths of  $B^\pm(K)$  are also studied by using various nuclear reactions [6,14,15].

The  $\tau^-$  strengths in the intermediate nucleus  ${}^A_{Z+1}\text{X}_2$  are mostly in the giant resonances, and there are small strengths at the 2QP and ground states. Likewise, the DBD ( $\tau^-\tau^-$ ) strengths are considered to be mostly in the double giant resonances, and there are small DBD strengths at the 2QP and ground states (Fig. 1). Double charge-exchange reactions on  ${}^A_{Z+1}\text{X}_1$  are used to study the DBD strengths in  ${}^A_{Z+2}\text{X}_3$  [6,49]. The double GT and SD giant-resonance energies measured from the ground state of  ${}^A_{Z+1}\text{X}_1$  are around  $E_G(\text{DGT}) = 26-32$  MeV and  $E_G(\text{DSD}) = 42-48$  MeV for DBD nuclei with  $A = 76-136$ . The ( ${}^{11}\text{B}$ ,  ${}^{11}\text{Li}$ ) data at Research Center for Nuclear Physics Osaka [50] show that most of the strengths are at the high-excitation-energy region. The double GT strengths for the DGT states are shown to have a positive correlation with the ground-state DBD-NMEs [51].

The delta isobar ( $\Delta$ ) is strongly excited by the quark  $\sigma\tau$  flip in a nucleon to form the  $N^{-1}\Delta$  giant resonance. Then the axial-vector  $M^\pm(K)$  and the axial-vector  $M_\alpha^{0\nu}$  with  $\alpha = \text{GT}$  and  $\text{T}$  are reduced with respect to the model NMEs without the  $\Delta$  isobar effect, which is incorporated by using the effective coupling of  $g_A^{\text{eff}}$  [6,52-55]. Studies of the  $N^{-1}\Delta$  effects are interesting.

In conclusion, the present work shows for the first time (i) a clear relation between the experimental SD strength distribution in the intermediate nucleus and the DBD NME in the pnQRPA formalism based on the SD data and (ii) a simple expression of  $M^{0\nu}$  as a function of  $A$  on the basis of the pnQRPA with the  $g_A^{\text{eff}}/g_A$  derived experimentally. Thus such experimental inputs are useful for pinning down the values for the DBD NMEs.

- 
- [1] H. Ejiri, *J. Phys. Soc. Jpn.* **74**, 2101 (2005).  
[2] F. T. Avignone, III, S. R. Elliott, and J. Engel, *Rev. Mod. Phys.* **80**, 481 (2008).  
[3] J. Vergados, H. Ejiri, and F. Šimkovic, *Rep. Prog. Phys.* **75**, 106301 (2012).  
[4] H. Ejiri and J. I. Fujita, *Phys. Rep.* **38**, 85 (1978).  
[5] H. Ejiri, *Phys. Rep.* **338**, 265 (2000).  
[6] H. Ejiri, J. Suhonen, and K. Zuber, *Phys. Rep.* **797**, 1 (2019).  
[7] J. Suhonen and O. Civitarese, *Phys. Rep.* **300**, 123 (1998).  
[8] A. Faessler and F. Simkovic, *J. Phys. G: Nucl. Part. Phys.* **24**, 2139 (1998).  
[9] J. Suhonen and O. Civitarese, *J. Phys. G: Nucl. Part. Phys.* **39**, 085105 (2012).  
[10] J. Barea, J. Kotila, and F. Iachello, *Phys. Rev. C* **87**, 014315 (2013).  
[11] J. Engel and J. Menéndez, *Rep. Prog. Phys.* **80**, 046301 (2017).  
[12] L. Jokiniemi, H. Ejiri, D. Frekers, and J. Suhonen, *Phys. Rev. C* **98**, 024608 (2018).  
[13] J. Detwiler, *Proc. Neutrino 2020* (2020), <https://conferences.fnal.gov/nu2020/>.  
[14] H. Ejiri, *Universe* **6**, 225 (2020).  
[15] H. Ejiri, *Front. Phys.* **9**, 650421 (2021).  
[16] H. Ejiri, N. Soukouti, and J. Suhonen, *Phys. Lett. B* **729**, 27 (2014).  
[17] J. Suhonen, *Phys. Rev. C* **96**, 055501 (2017).  
[18] J. T. Suhonen, *Front. Phys.* **5**, 55 (2017).  
[19] H. Ejiri, *Front. Phys.* **7**, 30 (2019).  
[20] F. Simkovic, V. Rodin, A. Faessler, and P. Vogel, *Phys. Rev. C* **87**, 045501 (2013).  
[21] J. Suhonen, *From Nucleons to Nucleus: Concepts of Microscopic Nuclear Theory* (Springer, Berlin, 2007).  
[22] H. Akimune *et al.*, *Phys. Lett. B* **394**, 23 (1997); **665**, 424 (2011).  
[23] J. H. Thies, D. Frekers, T. Adachi, M. Dozono, H. Ejiri, H. Fujita, Y. Fujita, M. Fujiwara, E.-W. Grewe, K. Hatanaka, P. Heinrichs, D. Ishikawa, N. T. Khai, A. Lennarz, H. Matsubara, H. Okamura, Y. Y. Oo, P. Puppe, T. Ruhe, K. Suda, A. Tamii, H. P. Yoshida, and R. G. T. Zegers, *Phys. Rev. C* **86**, 014304 (2012).  
[24] J. H. Thies, P. Puppe, T. Adachi, M. Dozono, H. Ejiri, D. Frekers, H. Fujita, Y. Fujita, M. Fujiwara, E. W. Grewe, K. Hatanaka, P. Heinrichs, D. Ishikawa, N. T. Khai, A. Lennarz, H. Matsubara, H. Okamura, Y. Y. Oo, T. Ruhe, K. Suda, A. Tamii,

- H. P. Yoshida, and R. G. T. Zegers, *Phys. Rev. C* **86**, 054323 (2012).
- [25] P. Puppe, D. Frekers, T. Adachi, H. Akimune, N. Aoi, B. Bilgier, H. Ejiri, H. Fujita, Y. Fujita, M. Fujiwara, E. Ganioglu, M. N. Harakeh, K. Hatanaka, M. Holl, H. C. Kozler, J. Lee, A. Lennarz, H. Matsubara, K. Miki, S. E. A. Orrigo, T. Suzuki, A. Tamii, and J. H. Thies, *Phys. Rev. C* **84**, 051305(R) (2011).
- [26] J. H. Thies, T. Adachi, M. Dozono, H. Ejiri, D. Frekers, H. Fujita, Y. Fujita, M. Fujiwara, E. W. Grewe, K. Hatanaka, P. Heinrichs, D. Ishikawa, N. T. Khai, A. Lennarz, H. Matsubara, H. Okamura, Y. Y. Oo, P. Puppe, T. Ruhe, K. Suda, A. Tamii, H. P. Yoshida, and R. G. T. Zegers, *Phys. Rev. C* **86**, 044309 (2012).
- [27] P. Puppe, A. Lennarz, T. Adachi, H. Akimune, H. Ejiri, D. Frekers, H. Fujita, Y. Fujita, M. Fujiwara, E. Ganioglu, E. W. Grewe, K. Hatanaka, R. Hodak, C. Iwamoto, N. T. Khai, A. Okamoto, H. Okamura, P. P. Povinec, G. Susoy, T. Suzuki, A. Tamii, J. H. Thies, and M. Yosoi, *Phys. Rev. C* **86**, 044603 (2012).
- [28] H. Ejiri and D. Frekers, *J. Phys. G: Nucl. Part. Phys.* **43**, 11LT01 (2016).
- [29] H. Akimune *et al.*, *J. Phys. G: Nucl. Part. Phys.* **47**, 05LT01 (2020).
- [30] H. Ejiri, *J. Phys. G: Nucl. Part. Phys.* **46**, 125202 (2019).
- [31] H. Ejiri and J. Suhonen, *J. Phys. G: Nucl. Part. Phys.* **42**, 055201 (2015).
- [32] J. Suhonen, *Phys. Lett. B* **607**, 87 (2005).
- [33] D. J. Horen *et al.*, *Phys. Lett. B* **99**, 383 (1981).
- [34] N. Yoshida and F. Iachello, *Prog. Theor. Exp. Phys.* **2013**, 043D01 (2013).
- [35] P. Pirinen and J. Suhonen, *Phys. Rev. C* **91**, 054309 (2015).
- [36] H. Ejiri, *J. Phys. G: Nucl. Part. Phys.* **44**, 115201 (2017).
- [37] A. Bohr and B. Mottelson, *Nuclear Structure, II* (W. A. Benjamin, Amsterdam, 1975).
- [38] H. Ejiri and M. A. deVoigt, *Electron and Gamma-ray Spectroscopy in Nuclear Physics* (Oxford University Press, Oxford, England, 1988).
- [39] P. Gysbers *et al.*, *Nat. Phys.* **15**, 428 (2019).
- [40] E. A. Coello Perez, J. Menéndez, and A. Schwenk, *Phys. Rev. C* **98**, 045501 (2018).
- [41] F. Šimkovic, R. Dvornický, D. Stefanik, and A. Faessler, *Phys. Rev. C* **97**, 034315 (2018).
- [42] L. Coraggio, L. De Angelis, T. Fukui, A. Gargano, N. Itaco, and F. Nowacki, *Phys. Rev. C* **100**, 014316 (2019).
- [43] J. Menéndez, D. Gazit, and A. Schwenk, *Phys. Rev. Lett.* **107**, 062501 (2011).
- [44] L. Jokiniemi and J. Suhonen, *Phys. Rev. C* **96**, 034308 (2017).
- [45] I. H. Hashim, H. Ejiri, T. Shima, K. Takahisa, A. Sato, Y. Kuno, K. Ninomiya, N. Kawamura, and Y. Miyake, *Phys. Rev. C* **97**, 014617 (2018).
- [46] L. Jokiniemi, J. Suhonen, H. Ejiri, and I. H. Hashim, *Phys. Lett. B* **794**, 143 (2019).
- [47] L. Jokiniemi and J. Suhonen, *Phys. Rev. C* **100**, 014619 (2019).
- [48] F. Šimkovic, R. Dvornický, and P. Vogel, *Phys. Rev. C* **102**, 034301 (2020).
- [49] F. Cappuzzello *et al.*, *Eur. Phys. J. A* **51**, 145 (2015).
- [50] K. Takahisa, H. Ejiri *et al.*, [arXiv:1703.08264](https://arxiv.org/abs/1703.08264)[nucl.exp].
- [51] N. Shimizu, J. Menendez, and K. Yako, *Phys. Rev. Lett.* **120**, 142502 (2018).
- [52] A. Bohr and B. R. Mottelson, *Phys. Lett. B* **100**, 10 (1981).
- [53] H. Ejiri, *Phys. Rev. C* **26**, 2628 (1982).
- [54] G. Cattapan and L. S. Ferreira, *Phys. Rep.* **362**, 303 (2002).
- [55] H. Ejiri, *Few-Body Syst.* **62**, 60 (2021).